

# Scaling description of the yielding transition in soft amorphous solids at zero temperature

Jie Lin <sup>\*</sup>, Edan Lerner <sup>\*</sup>, Alberto Rosso <sup>†</sup>, and Matthieu Wyart <sup>\*</sup>

<sup>\*</sup>Center for Soft Matter Research, Department of Physics, New York University, New York, NY 10003, and <sup>†</sup>Laboratoire de Physique Théorique et Modèles Statistiques (UMR CNRS 8626), Université de Paris-Sud, Orsay Cedex, France

Submitted to Proceedings of the National Academy of Sciences of the United States of America

**Yield stress materials flow if a sufficiently large shear stress is applied. Although such materials are ubiquitous and relevant for industry, there is no accepted microscopic description of how they yield, even in the simplest situation where temperature is negligible. Here we propose a scaling description of the yielding transition in amorphous solids made of soft particles at zero temperature. Our description makes a connection between the Herschel-Bulkley exponent characterizing the singularity of the flow curve near the yield stress  $\Sigma_c$ , the statistics and length scale of avalanches of plasticity at  $\Sigma_c$ , and the density  $P(x)$  of soft spots, or shear transformation zones, as a function of their distance  $x$  to an instability. We propose three scaling relations, and argue that all exponents characterizing these properties can be expressed in terms of three exponents  $\theta$ ,  $d_f$  and  $z$  characterizing respectively the density of soft spots, the fractal dimension of the avalanches, and their duration. Our description shares some similarity with the depinning transition that occurs when an elastic manifold is driven through a random potential, but also presents some striking differences. We test our three scaling relations in an elasto-plastic model, an automaton model similar to those used in depinning, but with a different interaction kernel, and find satisfying agreement with our predictions both in two and three dimensions.**

term | term | term

## Introduction

All solids will flow and behave as fluids if a sufficiently large shear stress is applied. In crystals, plasticity is governed by the motion of dislocations [1, 2, 3]. In amorphous solids there is no order, and conserved defects cannot be defined. However, as noticed by Argon [4], plasticity consists of elementary events localized in space, called shear transformations, where a few particles rearrange. This observation supports that there are special locations in the sample, called shear transformation zones or STZ's [5], where the system lies close to an elastic instability. Several theoretical approaches of plasticity, such as STZ theory [5, 6] or Soft Glassy Rheology (SGR) [7] assume that such zones relax independently, or are coupled to each other via an effective temperature. However, at zero temperature and small applied strain rate  $\dot{\gamma}$ , computer experiments [8, 9, 10, 11, 12, 13] and very recent experiments [14, 15] indicate that local rearrangements are not independent: plasticity occurs via avalanches in which many shear transformations are involved, forming elongated structures where plasticity localizes. At these small strain rates, one finds that the flow curves are singular, and follow a Herschel-Bulkley law  $\Sigma - \Sigma_c \sim \dot{\gamma}^{1/\beta}$  [16, 17]. These features are qualitatively reproduced by elastoplastic models [18, 19, 20, 21, 22, 23] where space is discretized. In these models, a site that yields plastically affects the stress in its surrounding via some interaction kernel  $\mathcal{G}(r)$ , argued to decay as a dipole and to display a four-fold symmetry [24, 25], as supported by observations [26, 27, 28, 29]. This perturbation can trigger novel plastic events and lead to avalanches. However, even within this picture, the relationship between the avalanche dynamics and the singularity of the flow curves remains debated [9, 30].

It is tempting to seek progress by building a comparison between the yielding transition and the much better understood depinning transition that occurs when an elastic interface is driven in a random environment [31, 2]. Both phenomena display very similar properties: near the depinning threshold force  $F_c$ , the velocity  $v$  vanishes non-analytically  $v \sim (F - F_c)^\beta$ , with  $\beta < 1$ , and the interplay between disorder and elasticity at threshold leads to broadly distributed avalanches corresponding to jerky motions of the interface. Much more is known about the depinning transition: it is a dynamical critical point, whose scaling relationships are well established and implies that the dynamics is ultimately controlled by two exponents, characterizing the roughness of the interface and the duration of the avalanches [31, 32]. These exponents, computed exactly above the critical dimension  $d_c$ , and perturbatively below  $d_c$  up to the second order in the parameter  $d_c - d$  [33, 34, 35] have been numerically evaluated with high precision [36].

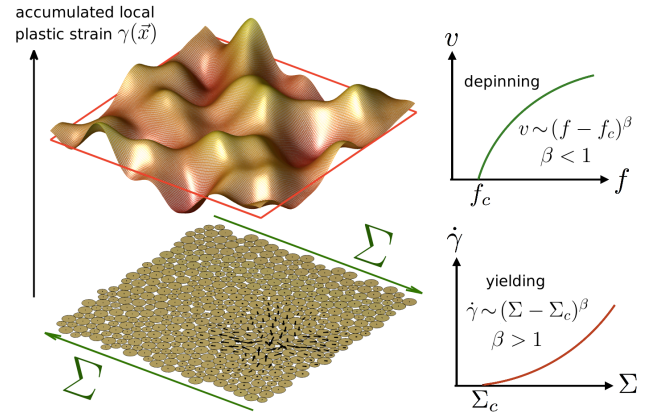


Fig. 1: Left: Analogy between the yielding transition of a  $d$ -dimensional amorphous solid and the depinning transition of an elastic interface of  $d$  dimensions in a space of  $d + 1$  dimensions, illustrated here for  $d = 2$ . The height of the interface is the accumulated local plastic strain generated by local plastic rearrangements; one example of the latter appears in the bottom. Right: the strain rate-stress (velocity-force) curves for the yielding (depinning) transition with  $\beta > 1$  ( $\beta < 1$ ) in yielding (depinning) transition.

Reserved for Publication Footnotes

Formally, elastoplastic models are very similar to automaton models known to capture well the depinning transition [19], as recalled below. The key difference is the interaction kernel  $\mathcal{G}$ , which for depinning is essentially a laplacian for short-range elasticity. This correspondence leads to an analogy between the depinning of an interface of dimension  $d$  in a  $d + 1$  dimensional space, and the yielding transition in  $d$  dimensions. The role that transverse displacements play in depinning corresponds to the local accumulated plastic strain  $\gamma(\vec{x})$  and the plastic strain  $\gamma$  can be identified with the center of mass of the interface, as illustrated in Fig.(1). This analogy has led to the proposition that the yielding transition is in the universality class of mean-field depinning [37, 38]. However, some intriguing finite size effects differ from depinning [12, 39, 11, 40]. We have recently explained these effects [23], showing that because the interaction kernel  $\mathcal{G}$  is long-range and of variable sign, the distribution of shear transformation zones at a distance  $x$  from instability,  $P(x)$ , is singular with  $P(x) \sim x^\theta$ , unlike in depinning for which  $\theta = 0$ . As we shall recall this singularity naturally explains these finite size effects. In this letter we argue that once this key difference with depinning is taken into account, the analogy between these two phenomena is fruitful, and leads to a scaling description of the yielding transition in terms of three exponents.

## Definition of exponents

*Flow curves:* Rheological properties are singular near the yielding transition. Herschel and Bulkley noticed [41] that for many yield stress materials,  $\Sigma = \Sigma_c + A\dot{\gamma}^n$ , where  $\dot{\gamma}$  is the macroscopic strain rate and  $\Sigma$  is the external shear stress. By analogy with depinning we instead introduce the exponent  $\beta = 1/n$ , such that

$$\dot{\gamma} \sim (\Sigma - \Sigma_c)^\beta. \quad [1]$$

In contrast to depinning,  $\beta > 1$  in the yielding transition.

*Length scales:* near the yielding transition the dynamics becomes more and more cooperative, and is correlated on a length scale  $\xi$ :

$$\xi \sim |\Sigma - \Sigma_c|^{-\nu} \quad [2]$$

*Avalanche statistics:* At threshold  $\Sigma = \Sigma_c$  the dynamics occur by avalanches of  $S$  localized plastic events, whose distribution  $\rho(S)$  follows a power-law:

$$\rho(S) \sim S^{-\tau} \quad [3]$$

$S$  can be defined as  $S = \Delta\gamma L^d$ , where  $\Delta\gamma$  is the plastic strain increment due to the avalanche, and  $L^d$  is the volume of the system.

Another important feature is the fractal dimension  $d_f$  of avalanches. Near the depinning transition, this quantity is related to the roughness of the elastic interface [31, 42]. Here instead,  $d_f$  can be defined by shearing the system quasi-statically, implying that  $\Sigma = \Sigma_c$ . For an infinite system, this would lead to power-law avalanches. However in a finite system of size  $L$ , this distribution is cut-off at some value  $S_c$ , where the linear extension of the avalanche is of order  $L$ , enabling to measure the scaling relation:

$$S_c \sim L^{d_f} \quad [4]$$

A key exponent relates length- and time- scales.  $z$  characterizes the duration  $T$  of an avalanche whose linear extension is  $L$ :

$$T \sim L^z \quad [5]$$

*Density of shear transformations:* If an amorphous solid is cut into small blocks containing several particles, one can define how much stress  $x_i$  needs to be applied to the block  $i$  before an instability occurs. The probability distribution  $P(x)$  is a measure of how many putative shear transformations are present in the sample [23]. Near the depinning transition, a similar quantity can be defined, and in that case it is well known that  $P(x) \sim x^0$  [31]. We have argued [23] that it must be so when the interaction kernel  $\mathcal{G}$  is *monotonic*, i.e. its sign is constant in space. For an elastic interface this is the case, as a region that yields will always destabilize other regions. This implies that locally the distance to instability  $x_i$  always decreases with time, until  $x_i < 0$  when the block  $i$  rearranges. Thus nothing in the dynamics allows the block  $i$  to forecast that an instability approaches, and no depletion nor accumulation is expected to occur near  $x_i = 0$ . By contrast for the yielding transition, the sign of  $\mathcal{G}$  varies in space. Thus locally  $x_i$  jumps both forward and backward, performing some kind of random walk. Since  $x = 0$  acts as an absorbing boundary condition (as the site is stabilized by a finite amount once it yields), one expects that depletion can occur near  $x = 0$ . In [23] we argued that  $P(x)$  must indeed vanish at  $x = 0$  if the interaction is sufficiently long-range (in particular if  $|\mathcal{G}| \sim 1/r^d$ , as is the case for the yielding transition), otherwise the system would be unstable: a small perturbation at the origin would cause extensive rearrangements in the system. Thus the yielding transition is affected by an additional exponent  $\theta$  that does not enter in the phenomenology of in the depinning problem:

$$P(x) \sim x^\theta \quad [6]$$

with  $\theta > 0$ . Using elastoplastic models we previously measured  $\theta \approx 0.4$  for  $d = 3$  and  $\theta \approx 0.6$  for  $d = 2$  [23], as we confirm here with improved statistics.

The definitions of the relevant exponents are summarized in Table 1, and their values as reported in the literature in Table 2.

## Scaling relations

We now propose several scaling relations, which essentially mirror arguments made in the context of the depinning transition (see supplementary information (S.I.)), with the additional feature that  $P(x)$  is singular.

*Stationarity:* Consider applying a quasi-static strain in a system of linear size  $L$ , as represented in Fig.(2). The stress  $\Sigma$  fluctuates due to avalanches: an avalanche of size  $S$  leads to a stress drop proportional to the plastic strain  $\Delta\gamma \sim S/L^d$ , of average  $\langle S \rangle/L^d$ . Using Eqs.(3,4) and assuming  $2 > \tau > 1$  one gets  $\langle S \rangle \sim L^{d_f(2-\tau)}$ , so that the average drop of stress is of order  $L^{d_f(2-\tau)-d}$ .

In between plastic events, the system loads elastic energy, and stress rises by some typical amount  $\Delta\Sigma$ .  $\Delta\Sigma$  is limited by the next plastic event, and is thus inversely proportional to the rate at which avalanches are triggered. Although one might think that if the system is twice larger, a plastic event will occur twice sooner (implying  $\Delta\Sigma \sim 1/L^d$ ), this is not the case and  $\Delta\Sigma$  depends on system size with a non-trivial exponent [12, 39, 11, 40]. As argued in [39] one expects  $\Delta\Sigma$  to be of order  $x_{min}$ , the weakest site in the system. If the  $x_i$  are independent this implies that  $\Delta\Sigma \sim L^{-\frac{d}{\theta+1}}$ . In [39] it was argued based on local considerations that  $\theta = 1/2$ . Instead our recent work [23] implies that  $\theta$  is governed by the elastic interactions between plastic events, and remains a non-trivial exponent that depends on interaction range and spatial dimension.

Imposing that in a stationary state the average drop and jump of stress must be equal leads to  $L^{d_f(2-\tau)-d} \sim L^{-\frac{d}{\theta+1}}$ , leading to our first scaling relation:

$$\tau = 2 - \frac{\theta}{\theta+1} \frac{d}{d_f} \quad [7]$$

As discussed in S.I., a similar but not identical relation holds also for the depinning transition [31, 43].

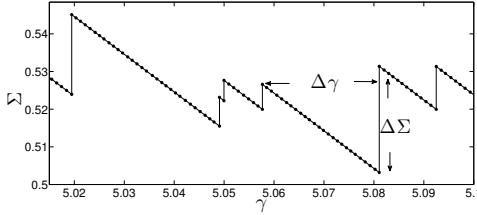


Fig. 2: Example of a stress  $\Sigma$  vs. plastic strain  $\gamma$  signal from quasi-static simulations of our elasto-plastic model. Avalanches relax the shear stress by some amount  $S/N$ .  $\Delta\Sigma$  is the stress increment needed to trigger a new avalanche. In the stationary state, these two quantities must be equal on the average.

*Dynamics:* A powerful idea in the context of the depinning transition is that avalanches below threshold and flow above threshold are intimately related [31]. Above threshold, the motion of the interface can be thought as consisting of a number of individual avalanches of spatial extension  $\xi$ , acting in parallel. We propose the same image for the yielding transition. If so, the strain rate  $\dot{\gamma}$  in the sample is simply equal to the characteristic strain rate of an avalanche of size  $\xi$ , leading to:

$$\dot{\gamma} = \frac{S}{T\xi^d} \sim (\Sigma - \Sigma_c)^{\nu(d+z-d_f)}. \quad [8]$$

implying our second scaling relation, which to our knowledge was not proposed in this context:

$$\beta = \nu(d+z-d_f) \quad [9]$$

*Statistical tilt symmetry:* If flow above  $\Sigma_c$  consists of independent avalanches of size  $\xi$ , then the avalanche-induced fluctuations of stress on that lengthscale,  $\delta\Sigma$ , must be of order:

$$\delta\Sigma \sim S_c/\xi^d \sim (\Sigma - \Sigma_c)^{\nu(d-d_f)} \quad [10]$$

One expects that the fluctuations of stress on the scale  $\xi$  must be of order of the distance to threshold  $\Sigma - \Sigma_c$ . Eq.(10) then leads to:

$$\nu = \frac{1}{d-d_f} \quad [11]$$

It was suggested in [40] that Eq.(11) may apply at the yielding transition. A similar relation holds for depinning of an interface if the elasticity is assumed to be linear, an assumption underlying Eq.(10). In that case it can be derived using the so-called statistical-tilt-symmetry. In S.I., we introduce and use this symmetry to justify the validity of Eq.(11) in elasto-plastic models of the yielding transition.

Overall the scaling relations Eqs.(7,15,11) allow to express the six exponents we have introduced in terms of three, which we choose to be  $\theta, d_f, z$ . The corresponding relations are indicated in Table 1.

## Elasto-plastic model

The phenomenological description proposed above may apply to real materials with inertial or over-damped dynamics, as well as to elasto-plastic models, although the yielding transition in these situations may not lie in the same universality class [40, 44]. In what follows we test our predictions in elasto-plastic models, implemented as in [23], whose details are recalled here.

We consider square ( $d=2$ ) and cubic ( $d=3$ ) lattices of unit lattice size with periodic boundary conditions, where each lattice point  $i$  can be viewed as the coarse grained description of a group of particles. It is characterized by a scalar stress  $\sigma_i$ , a local yield stress  $\sigma_i^{th}$ , and a strain  $\gamma_i = \gamma_i^{el} + \gamma_i^{pl}$ . The total stress carried by the system is  $\Sigma = \sum_i \sigma_i/L^d$ . The elastic strain satisfies  $\gamma_i^{el} \propto \sigma_i$ . The plastic strain is constant in time except when site  $i$  becomes plastic, which occurs at a rate  $1/\tau_c$  if the site is unstable, defined here as  $x_i \equiv \sigma_i^{th} - \sigma_i < 0$ . For simplicity we consider that  $\sigma_i^{th}$  does not vary in space, and use it to define our unit stress  $\sigma^{th} = 1$ .  $\tau_c$  is the only time scale in the problem, and defines our unit of time.

When plasticity occurs, the plastic strain increases locally and the stress is reduced by the same amount  $\delta\gamma_i^{pl} = -\delta\sigma_i = \delta x_i$ . We assume that  $\delta\gamma_i^{pl} = \sigma_i + \epsilon$  where  $\epsilon$  is some random number, taken to be uniformly distributed between  $-0.1$  and  $0.1$ .  $\epsilon = 0$  would correspond to imposing zero local stress after a plastic event (a choice that we avoid as it sometimes leads to periodic dynamics). When a site relaxes it affects the stress level on other sites immediately, such that:

$$\delta x_j = -\mathcal{G}(\vec{r}_{ij})\delta x_i \quad [12]$$

with  $\mathcal{G}(\vec{r}_{ij}) = \cos(4\phi)/r^2$  in an infinite two-dimensional system under simple shear, and where  $\phi$  is the angle between the shear direction and  $\vec{r}_{ij}$  [25]. In a finite system  $\mathcal{G}$  depends on the boundary conditions [25]. At fixed stress, by definition  $\mathcal{G}(0) = -1$  and stress conservation implies that the sum of  $\mathcal{G}$  on any line or column of the lattice is zero. At fixed global strain however, one plastic event reduces the stress by an amount of order  $1/L^d$ . When desired, we model

Table 1: The critical exponents and their expressions. The third column is the three scaling relations we derive in the text. We compare values measured in our elasto-plastic model both in 2d and 3d, with the predictions from the scaling relations.

exponent	expression	relations	2d measured/prediction	3d measured/prediction
$\theta$	$P(x) \sim x^\theta$		0.57	0.35
$z$	$T \sim l^z$		0.57	0.65
$d_f$	$S_c \sim L^{d_f}$		1.1	1.5
$\beta$	$\dot{\gamma} \sim (\Sigma - \Sigma_c)^\beta$	$\beta = 1 + z/(d-d_f)$	1.34/1.62	1.24/1.41
$\tau$	$\rho(S) \sim S^{-\tau}$	$\tau = 2 - \frac{\theta}{\theta+1} \frac{d}{d_f}$	1.36/1.34	1.43/1.48
$\nu$	$\xi \sim ( \Sigma - \Sigma_c )^{-\nu}$	$\nu = 1/(d-d_f)$	1.05/1.1	0.69/0.67

this effect by modifying the interaction kernel as follows:  $\mathcal{G}(\vec{r}_{ij}) \rightarrow \mathcal{G}(\vec{r}_{ij}) - 1/L^d$ .

In our model the average plastic strain is defined as  $\gamma = \frac{1}{L^d} \sum_i \gamma_i^{pl}$ , and the strain rate simply follows  $\dot{\gamma} = \sum_i \langle \delta \gamma_i^{pl} \rangle / L^d = \sum_i \sigma_i \Theta(\sigma_i - 1) / (\tau_c L^d)$ , where  $\Theta(x)$  is the heaviside function. At fixed stress above  $\Sigma_c$ , the system will get into a steady state with a finite  $\dot{\gamma}$ . Below or in the vicinity of  $\Sigma_c$  however, the system can spontaneously stop. If this occurs, we trigger the dynamics by giving very small random kicks to the system (chosen to conserve stress on every line and column) until one site becomes unstable. We do not include these arrested periods in our computation of strain rate.

This elasto-plastic model is essentially identical to the automaton models introduced in [45] in the context of the depinning transition, where the role of the plastic strain  $\gamma_i^{pl}$  is played by the transverse displacement of the elastic interface  $u_i$ . The only qualitative difference is the form of  $\mathcal{G}$ .

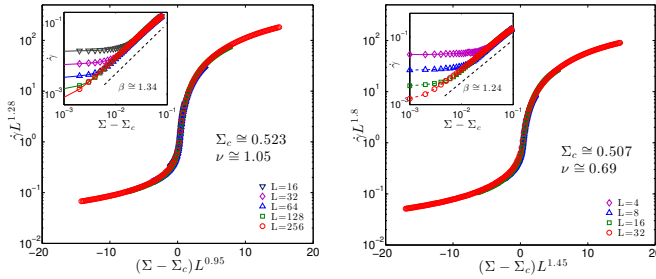


Fig. 3: Insets: flow curves  $\dot{\gamma}(\Sigma)$  in the vicinity of  $\Sigma_c$  for different system size  $L$  as indicated in legend in  $d = 2$  (left) and  $d = 3$  (right).  $\Sigma_c$  and the exponent  $\beta$  are estimated using a linear fit. Main curves: Scaling collapse of the flow curves  $\dot{\gamma}(\Sigma, L)$  after rescaling the axis according to Eq.(13), yielding the value of the exponent  $\nu$ .

### Numerical estimation of critical exponents

*Flow curves:* we first compute the flow curves  $\dot{\gamma}(\Sigma, L)$  at fixed stress  $\Sigma$  for various system size  $L$ . According to our scaling description we expect that:

$$\dot{\gamma} \sim L^{-\beta/\nu} f(L^{1/\nu}(\Sigma - \Sigma_c)) \quad [13]$$

where  $f$  is some scaling function. As shown in Fig.(3), we find that flow curves indeed collapse for a suitable rescaling of the axis. To obtain more precise exponents we first fit Eq.(1) directly for different system sizes, as shown in the inset of Fig.3. We find  $\beta \simeq 1.34$  and  $\Sigma_c \simeq 0.523$  for  $d = 2$ , and  $\beta \simeq 1.24$  and  $\Sigma_c \simeq 0.507$  for  $d = 3$ . From the rescaling of the axis leading to the collapse of Fig.(3), we extract  $\nu$  and find  $\nu \simeq 1.03$  for  $d = 2$  and  $\nu \simeq 0.69$  for  $d = 3$ .

*Avalanche statistics:* To study the statistics of avalanches while minimizing finite size effects, we work at constant stress  $\Sigma$ , and consider the evolution of  $\rho(S, \Sigma)$  as  $\Sigma \rightarrow \Sigma_c$ . We observe that the avalanche distribution display a power-law behavior below some cut-off  $S_c$ , as shown in Fig.(4). Fitting  $\rho(S) \sim S^{-\tau}$  we obtain  $\tau \simeq 1.36$  for  $d = 2$  and  $\tau \simeq 1.43$  for  $d = 3$ .

Next, to characterize the fractal dimension and the duration of avalanches, we use extremal dynamics: the stress is increased until an avalanche is triggered. During the avalanche the strain is fixed, and the stress decays. This method allows to study the quasi-static regime, and thus to stay at the critical point. Avalanches are cut-off at some characteristic value  $S_c$  for which the avalanche extension is

of order  $L$ , thus at large argument one expects  $\rho(S, L) \sim S^{-\tau} h(S/L^{d_f}) \sim L^{-d_f \tau} H(S/L^{d_f})$ , where  $h$  is some function and  $H(x) = x^{-\tau} h(x)$ . This collapse is checked in Fig.(5), and leads to  $d_f \approx 1.1$  for  $d = 2$  and  $d_f \approx 1.5$  for  $d = 3$ .

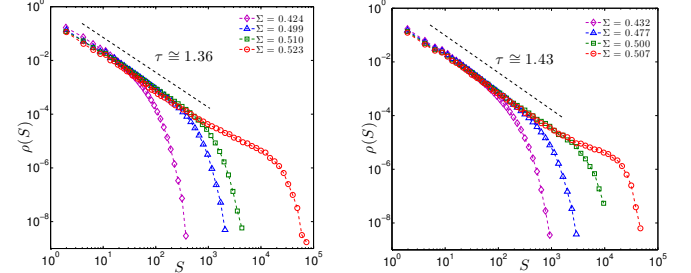


Fig. 4: Avalanche size distribution  $\rho(S)$  for different values of stress  $\Sigma$  as indicated in legend for (Left)  $d = 2$  and  $L = 256$  and (Right)  $d = 3$  and  $L = 32$ . A power-law behavior can be identified as  $\Sigma \rightarrow \Sigma_c$  from which the exponent  $\tau$  is inferred.

To measure the dynamical exponent we record, during extremal dynamics, the duration of each avalanche, and measure the duration distribution  $\rho(T)$  for different system size. These distributions are cut-off at some  $T_c$ , corresponding to the duration of the avalanches of spatial extension  $L$ , so that  $T_c \sim L^z$ . As shown in the right panels of Fig.(5) we indeed find a good collapse  $\rho(T, L) \sim T^{-\tau'} h_2(T/L^z) \sim L^{-\tau' z} H_2(T/L^z)$  with  $z \approx 0.57$ ,  $\tau' \approx 1.6$  for  $d = 2$  and  $z \approx 0.65$ ,  $\tau' \approx 1.9$  for  $d = 3$ .

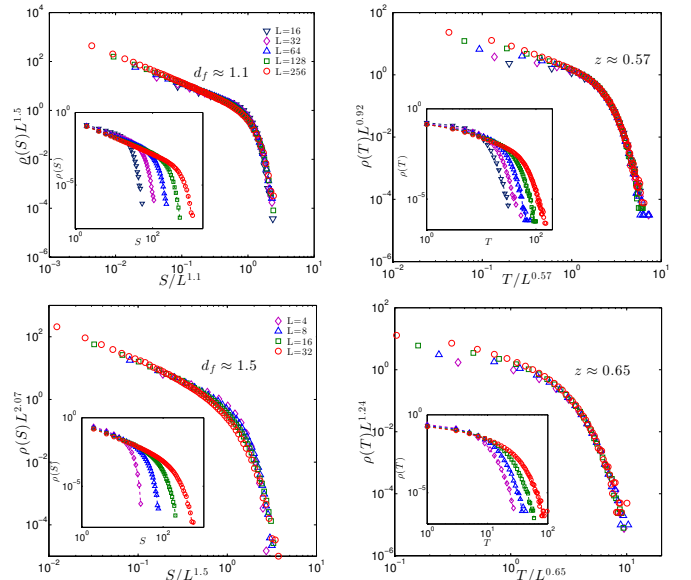


Fig. 5: Left, Insets: avalanche size distribution  $\rho(S, L)$  for quasi-static (extremal) dynamics as the system size  $L$  is varied in  $d = 2$  (upper curve) and  $d = 3$  (bottom curve). Main plots: rescaling avalanche size enable to collapse these distribution, allowing to extract a fractal dimension  $d_f$ . Right, Insets: distribution  $\rho(T)$  of the duration of the avalanches for the system sizes as indicated in legend in  $d = 2$  (upper curve) and  $d = 3$  (bottom curve). Main plots: The cut-off present in these distribution can be collapsed by rescaling time, leading to an estimate of the dynamical exponent  $z$ .

Table 2: Values of exponents as reported in the literature. The exponents characterizing the relationships between length and strain rate  $\xi \sim \dot{\gamma}^{-\nu/\beta}$ , average avalanche size and system length  $\langle S \rangle \sim L^{(2-\tau)d_f}$  and avalanche durations with sizes  $T \sim S^{z/d_f}$  are often reported, and are shown here. Three-dimensional observations are labeled (3d), otherwise the value correspond to two-dimensional systems.

exponent	values(2d)	values(3d)	lattice model	simulation	experiment
$\beta$	1.34	1.24	1.78[44]	1.17[37], 2[46]	2.22(3d)[47], 2.78[48], 2.22(3d)[49]
$\nu/\beta$	0.78	0.56	0.5[22], 0.6[44], 1[50]	0.5[9]	
$\tau$	1.36	1.43	1.34[51], 1.25[18], 1.5[37], 1.5[52]	1.3 [40], 1.3(3d)[40]	1.37–1.49(3d)[53]
$d_f$	1.1	1.5	1.5[50], 1.5[44], 1[18], 1[54]	0.9[40], 1.1(3d)[40]	
$(2-\tau)d_f$	0.7	0.8	0.75[18]	1[12], 0.6[40], 0.8(3d)[40]	
$z/d_f$	0.52	0.43	0.68[51], 0.5[38]	0.5[37]	
$\theta$	0.57	0.35		0.54[40], 0.43(3d)[40], 0.5[39], 0.5(3d)[39]	

**Density of shear transformations:** In elastoplastic models it is straightforward to access the local distance to thresholds  $x_i$  and to compute its distribution  $P(x)$  [23]. Here we recall these results with improved statistics. We fix the stress at  $\Sigma_c$ , and let the system evolve for a long enough time such that  $\gamma \gg 1$ . The dynamics occasionally stops; at that point we measure  $P(x)$ , and average over many realizations. As shown in Fig.(6), we find  $\theta \simeq 0.57$  for  $d = 2$ ,  $\theta \simeq 0.35$  for  $d = 3$ . Although in experiments  $P(x)$  is hard to access, the system size dependence of the average increment of stress where no plasticity occurs should be accessible, and follows  $\Delta\Sigma \sim L^{-d/(1+\theta)}$ . In the insets of Fig.(6)  $\Delta\Sigma$  is computed via extremal dynamics, leading to slightly smaller exponents  $\theta \simeq 0.50$  for  $d = 2$  and  $\theta \simeq 0.28$  for  $d = 3$ , a difference presumably resulting from corrections to scaling.

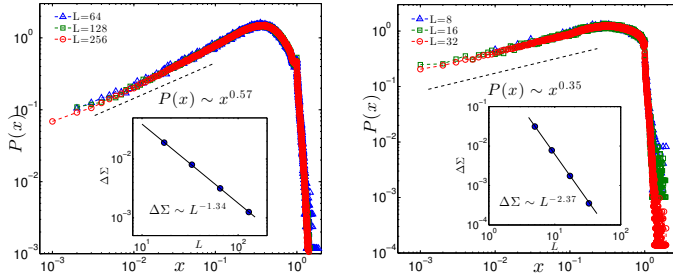


Fig. 6: Shear transformation distribution  $P(x)$  where  $x$  is the local distance to an instability for  $d = 2$  (left) and  $d = 3$  (right). Insets: amplitude of stress increments  $\Delta\Sigma$  before an instability occurs as a function of  $L$ , found to follow  $\Delta\Sigma \sim L^{-d/(1+\theta)}$ .

**Theory vs numerics.** Our scaling predictions can now be tested, and this comparison is shown in Table 1. We find excellent agreement for our predictions for  $\tau$  and  $\nu$ . For the exponent  $\beta$ , our numerics are close but somewhat lower than our predictions both in  $d = 2$  and  $d = 3$ , which we believe reflects the presence of large finite-size corrections to scaling expected with such long-range interactions.

### Elastoplastic model vs MD and experiments

Although elastoplastic models are well-suited to test theories, they make many simplifications, and thus may not fall in the universality class of real materials. One encouraging item is our estimate of  $\theta$ , which is very similar to the value extracted from finite size effects in MD simulations, as re-

ported in Table.2 under overdamped dynamics. This is consistent with our finding [23] that  $\theta$  (and  $\tau$ ) is independent of the choice of dynamical rules in our model, that can however dramatically affect the dynamics. Concerning the latter, our choice that the interaction is instantaneous in time, while still being long-range, is likely to affect the exponents  $z$  and  $\beta$ . We expect that if a more realistic time-dependent interaction kernel  $\mathcal{G}(\vec{r}, t)$  is considered (a costly choice numerically), the exponent  $z$  will satisfy  $z \geq 1$ . According to Eq.(15), this will lead to larger values of  $\beta$ , in agreement with experiments.

Finally in the overdamped MD simulations of [40],  $d_f = 0.9$  for  $d = 2$  and 1.1 for  $d = 3$ , according to Eq.(11) this supports that  $\nu < 2/d$  for  $d = 3$  - unlike what we find in our elasto-plastic model where this inequality is not supported. In the depinning problem, when  $\nu < 2/d$  another length scale enters in the scaling description, which affects in particular finite size effects [45, 55]. In this situation however, we expect our scaling description to be unchanged if  $\nu$  is meant to characterize the correlations of the dynamics for  $\Sigma > \Sigma_c$ .

### Conclusion

We have proposed a scaling description of stationary flow in soft amorphous solids, and it is interesting to reflect if this approach can apply to other systems. Plasticity in crystals shares many similarities with that of amorphous solids, and the far-field effect of a moving dislocation is essentially identical to the effect of a shear-transformation [2]. Thus we expect that the stability argument of [23] on the density of regions about to yield also applies in crystals, leading to a non-trivial exponent  $\theta$  in that case too. Our scaling relations may thus hold in crystals, although the formation of structures such as domain walls could strongly affect the yielding transition.

Despite the fact that avalanches of plasticity are seen in granular materials where particles are hard [14, 15], we believe that at least for over-damped systems, this behavior is only transient; and that the elasto-plastic description does not apply for such materials under continuous shear. Some of us have argued that in that case, a picture based on geometry applies [56, 57], which also leads to a diverging length scale, but of a different nature [58].

The scaling relations proposed here do not fix the values of the exponents, in particular that of  $\theta$ . To make progress, it is tempting to seek a mean-field description of this problem, that would apply beyond some critical dimension. Current mean-field models in which the interaction is random and does not decay with distance lead to  $\theta = 1$  [59, 23]. However, the anisotropy is lost in this view, and the fact that  $\theta$  diminishes as  $d$  increases when anisotropy is considered suggests that a mean-field model that includes anisotropy is needed. Such a model would be valuable to build a hydrodynamic description of flow, that would apply for example for slow flow near

walls [60, 61], a problem for which current descriptions do not include the role of anisotropy [62, 30].

1. M.-Carmen Miguel, Alessandro Vespignani, Stefano Zapperi, Jerome Weiss, and Jean-Robert Grasso. Intermittent dislocation flow in viscoplastic deformation. *Nature*, 410:667–671, April 2001.
2. Michael Zaiser. Scale invariance in plastic flow of crystalline solids. *Advances in Physics*, 55(1-2):185–245, 2006.
3. Karin A. Dahmen, Yehuda Ben-Zion, and Jonathan T. Uhl. Micromechanical model for deformation in solids with universal predictions for stress-strain curves and slip avalanches. *Phys. Rev. Lett.*, 102:175501, Apr 2009.
4. A.S Argon. Plastic deformation in metallic glasses. *Acta Metallurgica*, 27(1):47 – 58, 1979.
5. M. L. Falk and J. S. Langer. Dynamics of viscoplastic deformation in amorphous solids. *Phys. Rev. E*, 57:7192, 1998.
6. Eran Bouchbinder and JS Langer. Nonequilibrium thermodynamics of driven amorphous materials. iii. shear-transformation-zone plasticity. *Physical Review E*, 80(3):031133, 2009.
7. Peter Sollich. Rheological constitutive equation for a model of soft glassy materials. *Physical Review E*, 58(1):738, 1998.
8. C. E. Maloney and M. O. Robbins. Anisotropic Power Law Strain Correlations in Sheared Amorphous 2D Solids. *Physical review letters*, 102(22), JUN 5 2009.
9. Anael Lemaître and Christiane Caroli. Rate-Dependent Avalanche Size in Athermally Sheared Amorphous Solids. *Physical review letters*, 103(6), AUG 7 2009.
10. Smarajit Karmakar, Edan Lerner, Itamar Procaccia, and Jacques Zylberg. Statistical physics of elastoplastic steady states in amorphous solids: Finite temperatures and strain rates. *Phys. Rev. E*, 82(3):031301, Sep 2010.
11. K. Michael Salerno, Craig E. Maloney, and Mark O. Robbins. Avalanches in strained amorphous solids: Does inertia destroy critical behavior? *Phys. Rev. Lett.*, 109:105703, Sep 2012.
12. Craig Maloney and Anael Lemaître. Subextensive scaling in the athermal, quasistatic limit of amorphous matter in plastic shear flow. *Phys. Rev. Lett.*, 93:016001, Jul 2004.
13. F. Gimbert, D. Amitrano, J. Weiss, and G. Combe. From quasi-static to dense flow regime in compressed frictional granular media. *ArXiv e-prints*, August 2012.
14. Axelle Amon, Van Bau Nguyen, Ary Bruand, Jérôme Crassous, and Eric Clément. Hot spots in an athermal system. *Phys. Rev. Lett.*, 108:135502, Mar 2012.
15. Le Bouil Antoine, Amon Axelle, McNamara Sean, and Crassous Jérôme. Emergence of cooperativity in plasticity of soft glassy materials. *arXiv preprint arXiv:1402.7304*, 2014.
16. R Höhler and Sylvie Cohen-Addad. Rheology of liquid foam. *Journal of Physics: Condensed Matter*, 17(41):R1041, 2005.
17. Geraint P. Roberts and Howard A. Barnes. New measurements of the flow-curves for carboxyl dispersions without slip artefacts. *Rheologica Acta*, 40(5):499–503, 2001.
18. Mehdi Talamali, Viljo Petäjä, Damien Vandembroucq, and Stéphane Roux. Avalanches, precursors, and finite-size fluctuations in a mesoscopic model of amorphous plasticity. *Phys. Rev. E*, 84:016115, Jul 2011.
19. JC Baret, D Vandembroucq, and S Roux. Extremal model for amorphous media plasticity. *Physical review letters*, 89(19), NOV 4 2002.
20. Oğuz Umut Salman and Lev Truskinovsky. Minimal integer automaton behind crystal plasticity. *Phys. Rev. Lett.*, 106:175503, Apr 2011.
21. Kirsten Martens, Lydéric Bocquet, and Jean-Louis Barrat. Connecting diffusion and dynamical heterogeneities in actively deformed amorphous systems. *Phys. Rev. Lett.*, 106:156001, Apr 2011.
22. Guillemette Picard, Armand Ajdari, François Lequeux, and Lydéric Bocquet. Slow flows of yield stress fluids: Complex spatiotemporal behavior within a simple elastoplastic model. *Phys. Rev. E*, 71:010501, Jan 2005.
23. Jie Lin, Alaa Saade, Edan Lerner, Alberto Rosso, and Matthieu Wyart. On the density of shear transformations in amorphous solids. *EPL (Europhysics Letters)*, 105(2):26003, 2014.
24. J. D. Eshelby. The determination of the elastic field of an ellipsoidal inclusion, and related problems. *Proceedings of the Royal Society of London. Series A. Mathematical and Physical Sciences*, 241(1226):376–396, 1957.
25. G. Picard, A. Ajdari, F. Lequeux, and L. Bocquet. Elastic consequences of a single plastic event: A step towards the microscopic modeling of the flow of yield stress fluids. *The European Physical Journal E*, 15(4):371–381, 2004.
26. Craig E. Maloney and Anael Lemaître. Amorphous systems in athermal, quasistatic shear. *Phys. Rev. E*, 74:016118, Jul 2006.
27. Joyjit Chattoraj and Anael Lemaître. Elastic signature of flow events in supercooled liquids under shear. *Phys. Rev. Lett.*, 111:066001, Aug 2013.
28. Peter Schall, David A. Weitz, and Frans Spaepen. Structural rearrangements that govern flow in colloidal glasses. *Science*, 318(5858):1895–1899, 2007.
29. Pinshane Y. Huang, Simon Kurash, Jonathan S. Alden, Ashvini Shekhawat, Alexander A. Alemi, Paul L. McEuen, James P. Sethna, Ute Kaiser, and David A. Muller. Imaging atomic rearrangements in two-dimensional silica glass: Watching silica’s dance. *Science*, 342(6155):224–227, 2013.
30. Lydéric Bocquet, Annie Colin, and Armand Ajdari. Kinetic theory of plastic flow in soft glassy materials. *Phys. Rev. Lett.*, 103:036001, Jul 2009.
31. Daniel S. Fisher. Collective transport in random media: from superconductors to earthquakes. *Physics Reports*, 301(173):113 – 150, 1998.

**ACKNOWLEDGMENTS.** We thank Eric DeGiuli, Alaa Saade, Le Yan, Gustavo Düring, Bruno Andreotti and Daniel Fisher for discussions. MW acknowledges support from NYU Poly Seed Fund Grant M8769, NSF CBET Grant 1236378, NSF DMR Grant 1105387, and MRSEC Program of the NSF DMR-0820341 for partial funding.

32. Mehran Kardar. Nonequilibrium dynamics of interfaces and lines. *Physics reports*, 301(1):85–112, 1998.
33. Thomas Nattermann, Semjon Stepanow, Lei-Han Tang, and Heiko Leschhorn. Dynamics of interface depinning in a disordered medium. *Journal de Physique II*, 2(8):1483–1488, 1992.
34. Onuttom Narayan and Daniel S Fisher. Threshold critical dynamics of driven interfaces in random media. *Physical Review B*, 48(10):7030, 1993.
35. Pascal Chauve, Pierre Le Doussal, and Kay Jörg Wiese. Renormalization of pinned elastic systems: how does it work beyond one loop? *Physical review letters*, 86(9):1785, 2001.
36. Ezequiel E Ferrero, Sebastián Bustingorry, and Alejandro B Kolton. Nonsteady relaxation and critical exponents at the depinning transition. *Physical Review E*, 87(3):032122, 2013.
37. N. Goldenfeld G. Tsekenis, J. T. Uhl and K. A. Dahmen. Determination of the universality class of crystal plasticity. *Europhysics Letters*, 101, Feb 2013.
38. Karin A Dahmen, Yehuda Ben-Zion, and Jonathan T Uhl. A simple analytic theory for the statistics of avalanches in sheared granular materials. *Nature Physics*, 7(7):554–557, 2011.
39. Smarajit Karmakar, Edan Lerner, and Itamar Procaccia. Statistical physics of the yielding transition in amorphous solids. *Phys. Rev. E*, 82:055103, Nov 2010.
40. K. Michael Salerno and Mark O. Robbins. Effect of inertia on sheared disordered solids: Critical scaling of avalanches in two and three dimensions. *Phys. Rev. E*, 88:062206, Dec 2013.
41. WH Herschel and R Bulkley. Consistency measurements of rubber benzene solutions. *Koll. Zeit*, 39:291, 1926.
42. Alberto Rosso, Alexander K Hartmann, and Werner Krauth. Depinning of elastic manifolds. *Physical Review E*, 67(2):021602, 2003.
43. LE Aragón, EA Jagla, and A Rosso. Seismic cycles, size of the largest events, and the avalanche size distribution in a model of seismicity. *Physical Review E*, 85(4):046112, 2012.
44. Alexandre Nicolas, Kirsten Martens, Lydéric Bocquet, and Jean-Louis Barrat. Universal and non-universal features in coarse-grained models of flow in disordered solids. *arXiv preprint arXiv:1402.4655*, 2014.
45. Onuttom Narayan and A Alan Middleton. Avalanches and the renormalization group for pinned charge-density waves. *Physical Review B*, 49(1):244, 1994.
46. Pinaki Chaudhuri, Ludovic Berthier, and Lydéric Bocquet. Inhomogeneous shear flows in soft jammed materials with tunable attractive forces. *Phys. Rev. E*, 85:021503, Feb 2012.
47. Michel Cloitre, Régis Borrega, Fabrice Monti, and Ludwik Leibler. Glassy dynamics and flow properties of soft colloidal pastes. *Phys. Rev. Lett.*, 90:068303, Feb 2003.
48. M. E. Möbius, G. Katgert, and M. van Hecke. Relaxation and flow in linearly sheared two-dimensional foams. *EPL (Europhysics Letters)*, 90(4):44003, 2010.
49. Lydiane Bécu, Sébastien Manneville, and Annie Colin. Yielding and flow in adhesive and nonadhesive concentrated emulsions. *Phys. Rev. Lett.*, 96:138302, Apr 2006.
50. Kirsten Martens, Lydéric Bocquet, and Jean-Louis Barrat. Connecting diffusion and dynamical heterogeneities in actively deformed amorphous systems. *Phys. Rev. Lett.*, 106:156001, Apr 2011.
51. Zoe Budrikis and Stefano Zapperi. Avalanche localization and crossover scaling in amorphous plasticity. *Physical Review E*, 88(6):062403, 2013.
52. Clara B. Picallo, Juan M. López, Stefano Zapperi, and Mikko J. Alava. From brittle to ductile fracture in disordered materials. *Phys. Rev. Lett.*, 105:155502, Oct 2010.
53. B. A. Sun, H. B. Yu, W. Jiao, H. Y. Bai, D. Q. Zhao, and W. H. Wang. Plasticity of ductile metallic glasses: A self-organized critical state. *Phys. Rev. Lett.*, 105:035501, Jul 2010.
54. Michael Zaiser and Nikos Nikitas. Slip avalanches in crystal plasticity: scaling of the avalanche cut-off. *Journal of Statistical Mechanics: Theory and Experiment*, 2007(04):P04013, 2007.
55. Christopher R Myers and James P Sethna. Collective dynamics in a model of sliding charge-density waves. ii. finite-size effects. *Physical Review B*, 47(17):11194, 1993.
56. E. Lerner, G. Düring, and M. Wyart. Toward a microscopic description of flow near the jamming threshold. *EPL (Europhysics Letters)*, 99(5):58003, 2012.
57. Edan Lerner, Gustavo Düring, and Matthieu Wyart. A unified framework for non-brownian suspension flows and soft amorphous solids. *Proceedings of the National Academy of Sciences*, 109(13):4798–4803, 2012.
58. Gustavo Düring, Edan Lerner, and Matthieu Wyart. Length scales and self-organization in dense suspension flows. *Phys. Rev. E*, 89:022305, Feb 2014.
59. P. Hébraud and F. Lequeux. Mode-coupling theory for the pasty rheology of soft glassy materials. *Phys. Rev. Lett.*, 81:2934–2937, Oct 1998.
60. Y. Forterre and O. Pouliquen. Flows of dense granular media. *Annual Review of Fluid Mechanics*, 40:1–24, 2008.
61. J Goyon, A Colin, G Ovarlez, A Ajdari, and L Bocquet. Spatial cooperativity in soft glassy flows. *Nature*, 454(7200):84–87, 2008.
62. Ken Kamrin and Georg Koval. Nonlocal constitutive relation for steady granular flow. *Phys. Rev. Lett.*, 108:178301, Apr 2012.



# Supplementary Material

## General scaling relations

The three scaling relations derived in the main text for the critical exponents of the yielding transition are similar but not identical to the scaling relations obtained for the depinning transition of an elastic interface. In the following we derive three more general relations, namely

$$\nu = \frac{1}{\alpha_k + d - d_f} \quad [14]$$

$$\beta = \nu(d - d_f + z) \quad [15]$$

$$\tau = 2 - \frac{d_f - d + 1/\nu}{d_f} - \frac{\theta}{\theta + 1} \frac{d}{d_f} \quad [16]$$

that hold both for yielding and depinning. Here  $\alpha_k$  is the dimension of the interaction kernel  $\mathcal{G}$ . The first relation is guaranteed only in presence of statistical-tilt-symmetry, hence only when the interactions are linear, while the other two relations are expected to be very general. In the context of the yielding transition  $\alpha_k = 0$  and  $d_f < d$  so that  $\beta > 1$ . In the context of the depinning transition  $\theta = 0$  and  $d_f \geq d$ , the dimension of the interaction kernel is  $\alpha_k = 2$  for short range elasticity and  $\alpha_k = 1$  for the long range elasticity of the contact line of a liquid meniscus [1] or of the crack front in brittle materials [2, 3].

## From the elasto-plastic automaton to the continuum model.

The  $d$  dimensional elasto-plastic model studied in this paper is a discrete automaton. Its continuum limit gives the time evolution of the strain field  $\gamma_{\vec{r}}$  in each point of the space:

$$\partial_t \gamma_{\vec{r}} = \int_{\vec{r}'} \mathcal{G}(\vec{r} - \vec{r}') \gamma_{\vec{r}'} + \Sigma + \sigma^{\text{dis}}(\gamma_{\vec{r}}, \vec{r}) \quad [17]$$

The first term of the equation describes the interactions between the different parts of the system. Note that the interactions are linear in the strain field  $\gamma$ , and governed by a time-independent interaction kernel,  $\mathcal{G}(\vec{r})$ . As discussed in the main text, for elastic depinning models the kernel is monotonic, while for amorphous materials it is non-monotonic, anisotropic and can be conveniently written in the Fourier space:

$$\mathcal{G}(\vec{k}) = \begin{cases} -\frac{4k_x^2 k_y^2}{k^4}, & \text{for } d = 2 \\ -\frac{4k_x^2 k_y^2 + k_z^2 k^2}{k^4}, & \text{for } d = 3. \end{cases} \quad [18]$$

The other two terms are the external stress,  $\Sigma$ , and the quenched disorder,  $\sigma^{\text{dis}}(\gamma, \vec{r})$ , which takes into account the inhomogeneities of the local yield stress. In the automaton model the scalar stress  $\sigma_i$  corresponds to the sum of the first two terms, and  $\sigma^{\text{dis}}(\gamma, \vec{r})$  is assumed to be a collection of narrow wells randomly located along  $\vec{r}$ . The parameters  $\sigma^{th}$ ,  $\epsilon$  and  $\tau_c$  are related respectively to the well depth, to the distance between consecutive wells and to the time needed to move from an unstable well to a stable one.

Below threshold,  $\Sigma < \Sigma_c$ , the local strain fields are pinned inside a set of narrow wells. If a small perturbation is applied (e.g. a little change in the well locations), the local strain field responds either (almost everywhere) linearly simply readjusting its value inside the well, either (when a well

becomes unstable) with a large modification accompanied by a stress release that can be the seed of a large avalanche. This non-linear response gives a singular contribution to the susceptibility which becomes important close to  $\Sigma_c$ . Note that in presence of a non-monotonic interaction kernel, the avalanche size  $S = \sum_i \Delta\gamma_i$  can be positive or negative, however the positive external stress  $\Sigma$  strongly suppress negative avalanches that can, in practice, be neglected.

**The statistical tilt symmetry.** We now focus on the response of the system when we add to Eq.(17) a tilt,  $\sigma_{\vec{r}}^{\text{tilt}}$ , namely an inhomogeneous local stress of zero spatial average. In presence of linear interactions, the tilt can be absorbed in a new strain field  $\tilde{\gamma}_{\vec{r}}$  defined as

$$\tilde{\gamma}_{\vec{r}} = \gamma_{\vec{r}} + \int_{\vec{r}'} \mathcal{G}^{-1}(\vec{r} - \vec{r}') \sigma_{\vec{r}'}^{\text{tilt}} \quad [19]$$

and governed by the following evolution equation

$$\partial_t \tilde{\gamma}_{\vec{r}} = \int_{\vec{r}'} \mathcal{G}(\vec{r} - \vec{r}') \tilde{\gamma}_{\vec{r}'} + \Sigma + \sigma^{\text{dis}}(\tilde{\gamma} - \mathcal{G}^{-1} \sigma^{\text{tilt}}, \vec{r}). \quad [20]$$

The latter equation points out that the effect of the tilt can be absorbed with a shift of the location of the narrow wells. Thus, once the average over disorder is taken, the tilt disappears from Eq.(20) if the correlation  $\overline{\sigma^{\text{dis}}(\gamma, \vec{r}) \sigma^{\text{dis}}(\gamma', \vec{r}')}$  only depend on  $\gamma - \gamma'$ . For example in the steady state, when the system becomes independent of the initial conditions, the average response of  $\gamma_q$  to a tilt  $\sigma_q^{\text{tilt}}$  acting on the mode  $q$ , is

$$\chi_q = \frac{\overline{\partial \gamma_q}}{\partial \sigma_q^{\text{tilt}}} = \frac{\overline{\partial \tilde{\gamma}_q - \mathcal{G}_q^{-1} \sigma_q^{\text{tilt}}}}{\partial \sigma_q^{\text{tilt}}} = \mathcal{G}_q^{-1} \quad [21]$$

This exact expression should be compared with the scaling behaviour of the singular part of the susceptibility governed by the characteristic scale  $\xi \sim (\Sigma_c - \Sigma)^{-\nu}$ . In this regime the strain field grows as  $\Delta\gamma \simeq \xi^{d_f - d}$  and noting that the tilt has the dimension of a stress, we expect that the singular part of the susceptibility scales as  $\chi^{\text{sing}} \sim \xi^{1/\nu + d_f - d}$ , which gives  $1/\nu - d + d_f = \alpha_k$ , namely Eq.(14). Here  $\alpha_k$  is the dimension of the kernel  $1/\mathcal{G}_q$ . For short range elastic depinning  $\alpha_k = 2$ , for long range depinning  $\alpha_k = 1$ , while the anisotropic kernel one has  $\alpha_k = 0$ .

**Stationarity.** Concerning the other two scaling relations: Eq.(15) is identical to the one derived in the main text and Eq.(16) is still a consequence of the stationarity of the avalanche dynamics. In general an avalanche of size  $S$  leads to a stress drop which is not simply proportional to the plastic strain, but rather to  $\Delta\gamma L^{d - d_f - 1/\nu}$ , so that the average stress drop induced by avalanches scales as

$$\Delta\Sigma \sim \frac{\langle S \rangle}{L^d} \frac{L^{-1/\nu}}{L^{d_f - d}}. \quad [22]$$

On the other hand the stress injection before observing a new avalanche scales as  $L^{-d/(\theta+1)}$ , so that

$$\frac{\langle S \rangle}{L^d} \frac{L^{-1/\nu}}{L^{d_f - d}} \sim L^{-d/(\theta+1)}. \quad [23]$$

Finally, using  $\langle S \rangle \sim L^{(2-\tau)d_f}$  we obtain Eq.(16).

1. J. F. Joanny and P.G. De Gennes, *J. Chem. Phys.*, 81 552 (1984).
2. H. Gao and J. R. Rice, *J. Appl. Mech.*, 56 828 (1989).
3. D. Bonamy and E. Bouchaud, *Phys. Rep.*, 498 1 (2011).